

CHONDRULE FORMATION AND PROTOPLANETARY DISK HEATING BY CURRENT SHEETS IN NON-IDEAL MAGNETOHYDRODYNAMIC TURBULENCE

M. K. RYAN JOUNG^{1,2}, MORDECAI-MARK MAC LOW^{2,1}, AND DENTON S. EBEL³
Draft version October 30, 2018

ABSTRACT

We study magnetic field steepening due to ambipolar diffusion (Brandenburg & Zweibel 1994) in protoplanetary disk environments and draw the following conclusions. Current sheets are generated in magnetically active regions of the disk where the ionization fraction is high enough for the magnetorotational instability to operate. In late stages of solar nebula evolution, the surface density is expected to have lowered and dust grains to have gravitationally settled to the midplane. If the local dust-to-gas mass ratio near the midplane is increased above cosmic abundances by factors $\gtrsim 10^3$, current sheets reach high enough temperatures to melt millimeter-sized dust grains, and hence may provide the mechanism to form meteoritic chondrules. In addition, these current sheets possibly explain the near-infrared excesses observed in spectral energy distributions (SEDs) of young stellar objects. Direct imaging of protoplanetary disks via a nulling interferometer or, in the future, a multi-band, adaptive optics coronagraph can test this hypothesis.

Subject headings: instabilities — meteors, meteoroids — MHD — planetary systems: protoplanetary disks — solar system: formation — turbulence

1. INTRODUCTION

Chondrules are millimeter-sized silicate spheres with igneous textures embedded in the most common type of meteorites, comprising 50–80 % of their mass. Their formation is a long-standing mystery in solar system formation. Radioisotope datings place them among the first solids to have condensed out of the slowly cooling solar nebula. As such, they represent the remains of early materials that later formed the terrestrial planets. Their nearly spherical shapes and glassy compositions indicate that they cooled within a few hours after being molten, but not in the few seconds that objects that size would cool in free space. The associated heating event, whatever the origin, must have been transient and localized as evidenced by the inferred rapid heating and cooling rates, and the observed retention of volatiles such as sulfur (which vaporizes by prolonged heating above 650 K). To explain the high abundance of chondrules, it must have been a widespread phenomenon. Hence, encrypted in chondrules are important clues to physical conditions that prevailed in the early stages of solar system formation. Some even argue that taking the form of millimeter-sized molten spheres is a necessary intermediate step for initially micron-sized dust grains to grow to kilometer-sized objects (Hewins 1997).

A successful theory of chondrule formation should at least meet the following constraints: (1) the extremely short heating timescale of roughly seconds to minutes (Connolly & Love 1998), (2) the cooling rate of 10^2 – 10^3 K hr⁻¹ (Radomsky & Hewins 1990; Lofgren & Lanier 1990), and (3) the narrow range of sizes (0.1–1 mm), inferred from laboratory analyses of textures and compositions as well as from attempts to reproduce chondrules. In addition, many chondrules show evidences of multiple

heating events, so the heating event must have occurred more than once. Since the initial discovery 200 years ago (Howard 1802), their formation process has received considerable attention in both meteoritics and solar system astronomy, yet it remains elusive (Wood 1996). Proposed mechanisms in the past (see the summary by Boss 1996, for the pros and cons) include nebula shocks, lightning, and an X-wind. None of these mechanisms have really been widely accepted (Hewins 1996), although recent work on shock heating by Desch & Connolly (2002) has gained wide attention.

Infrared observations and subsequent theoretical modeling of T Tauri stars revealed the existence of circumstellar (protoplanetary) disks (Mendoza 1968; Shu, Adams, & Lizano 1987; Adams, Lada, & Shu 1987; Beckwith et al. 1990), many of which are actively accreting (see, e.g. the review by Calvet, Hartmann, & Strom 2000). These systems are generally thought to be analogs of the early solar nebula. On the theoretical side, magnetorotational instability (MRI) provided a solution to the long-standing problem of identifying the cause of anomalous viscosity, which allows mass accretion of the disk (Balbus & Hawley 1991; Hawley & Balbus 1991, collectively referred to as BH91 hereafter). When applied to partially ionized disks, it remains an efficient mechanism of generating turbulence as long as ions are sufficiently well-coupled to neutrals, i.e., if ion-neutral collision rate far exceeds the orbital rotation rate: $\nu_{in} \gg \Omega$ (Blaes & Balbus 1994; Mac Low et al. 1995; Hawley & Stone 1998). In the case of protoplanetary disks, however, a large portion, especially near the disk midplane, is associated with relatively low ionization fraction ($\sim 10^{-12}$), and hence thought to be magnetically dead (Gammie 1996; Glassgold, Najita, & Igea 1997).

In partially ionized disks, ambipolar diffusion arises be-

¹ Department of Astronomy, Columbia University, 550 West 120th Street, New York, NY 10027; moo@astro.columbia.edu

² Department of Astrophysics, American Museum of Natural History, 79th Street at Central Park West, New York, NY 10024; mordecai@amnh.org

³ Department of Earth and Planetary Sciences, American Museum of Natural History, 79th Street at Central Park West, New York, NY 10024; debel@amnh.org

cause magnetic forces act on the charged component, i.e. ions, only (Mestel & Spitzer 1956). As the ions drift through neutrals, the magnetic field lines drag the ions with them, steepening field gradients near magnetic nulls stretched by shear flows (Brandenburg & Zweibel 1994, hereafter BZ94). Consequently, sheets of high electric current form, as was confirmed by numerical simulations (Mac Low et al. 1995; Suzuki & Sakai 1996). BZ94 originally proposed this as a mechanism for rapid magnetic reconnection in the interstellar medium. Ambipolar diffusion is important in another context: as a heating source (Scalo 1977; Goldsmith & Langer 1978; Zweibel & Josafatsson 1983; Elmegreen 1985). Recently, using three-dimensional simulations of turbulent, magnetized molecular clouds, Padoan, Zweibel, & Nordlund (2000) pointed out that ambipolar diffusion heating is a significant source of heating in molecular clouds and that it can be larger than the cosmic ray heating. In this paper, we examine the possibility that similar physics operates in protoplanetary disks, such as in the solar nebula that eventually became our solar system.

The purpose of this paper is twofold. First, we show that current sheets are generated in magnetically active regions within protoplanetary disks. We study the properties of these current sheets and determine when and where the associated heating becomes significant. Second, we apply this formalism to the following two unresolved issues: the heating mechanism that melted chondrules in the early solar nebula and the near-infrared excesses observed in spectral energy distributions (SEDs) of young stellar objects.

We later demonstrate that the heating of dust grains by current sheets is ineffective for a standard model of the early solar nebula in which the dust-to-gas ratio $\zeta \simeq 0.01$. However, at lower gas densities and much higher dust-to-gas ratios than those usually assumed in the standard model, these current sheets are found to reach high enough temperatures to melt millimeter-sized dust grains. We propose that these unusual conditions occur near the midplane in late stages of solar nebula evolution, when the gas surface density has decreased due to various mechanisms discussed below, and dust grains have gravitationally settled. The surfaces of this dust-enriched midplane layer are then sufficiently dense and ionized to host thin ($l \approx 10^2$ km), hot ($T > 1600$ K) current sheets. Circulation of dust to the surface by turbulence within the dust layer is invoked to explain the observed high abundance of chondrules.

The basic features of our current sheet model are set forth in § 2. In § 3.1 we use this model to investigate a scenario in which chondrules are heated inside current sheets, solving numerically the coupled equations of energy transfer for gas and dust particles. The results are presented in § 3.2. We argue, in § 3.3, that in late stages of solar nebula evolution current sheets capable of melting most of the millimeter-sized dust particles form in the dust-rich midplane. In § 3.4 we discuss possible observational signatures of current sheets. Finally, in § 4 we list limitations of our model.

2. CURRENT SHEET MODEL

2.1. Basic Equations

The magnetic field evolves according to the induction equation,

$$\frac{\partial \mathbf{B}}{\partial t} = \nabla \times (\mathbf{v}_e \times \mathbf{B} - \eta \nabla \times \mathbf{B}), \quad (1)$$

where \mathbf{v}_e denotes the electron velocity and η is the associated resistivity given by

$$\eta = \frac{c^2}{4\pi\sigma_e} = \frac{234}{\chi_e} T_g^{1/2} \text{ cm}^2 \text{ s}^{-1} \quad (2)$$

(Krall & Trivelpiece 1973). Here, c is the speed of light, $\chi_e = n_e/n_n$ is the electron fraction, and T_g is the ambient gas temperature. For the last equality in Eqn. (2), we adopt the value of the electrical conductivity, σ_e , from Draine, Roberge, & Dalgarno (1983) and Blaes & Balbus (1994). Subscripts e , i , and n denote quantities pertaining to electron, ion, and neutral components, respectively. Other quantities of relevance in this paper are the mean mass per particle of $m_n = 2.33 m_p$, where m_p is the proton mass, and the mean ion mass of $m_i = 39 m_p$ at densities where ionized potassium, K^+ , is generally the dominant ion species (Balbus & Terquem 2001).

In the ideal MHD limit, the electron velocity is indistinguishable from the center-of-mass velocity of the fluid. This approximation breaks down in two ways as χ_e decreases. First, ions slip through neutrals, and for low enough χ_e , when ion pressure and inertia can be neglected, the strong coupling approximation can be used to compute the ambipolar drift velocity by balancing the Lorentz force $\mathbf{J} \times \mathbf{B}/c$ acting on the ions against the frictional drag $\rho_i \nu_{in}(\mathbf{v}_i - \mathbf{v}_n)$ arising from collisions with neutrals. Second, when ions and electrons move along a direction perpendicular to a magnetic field, they experience the Lorentz force acting normal to both directions but they drift away in two opposite directions due to the different signs of their electric charges. This causes the Hall effect. The electron velocity in a weakly ionized medium is then

$$\mathbf{v}_e = \mathbf{v} + (\mathbf{v}_i - \mathbf{v}) + (\mathbf{v}_e - \mathbf{v}_i) = \mathbf{v} + \frac{\mathbf{J} \times \mathbf{B}}{c\rho_i\nu_{in}} - \frac{\mathbf{J}}{n_e e}, \quad (3)$$

where $\rho_i = m_i n_i$ and $\nu_{in} = \gamma \rho_n$ are the ion mass density and ion-neutral collision rate. The value of the drag coefficient, $\gamma = 2.75 \times 10^{13} \text{ cm}^3 \text{ s}^{-1} \text{ g}^{-1}$ (Balbus & Terquem 2001). Since $\chi_e \ll 1$ in our case (see § 2.2), the neutral velocity is the same as the center-of-mass velocity, \mathbf{v} . The current density has the usual form $\mathbf{J} = (c/4\pi)\nabla \times \mathbf{B}$. We plug Eqn. (3) into Eqn. (1) and consider the case in which the currents and fields are perpendicular ($\mathbf{J} \cdot \mathbf{B} = 0$), so the induction equation becomes

$$\frac{\partial \mathbf{B}}{\partial t} = \nabla \times (\mathbf{v} \times \mathbf{B}) - \nabla \times \left[\left(\frac{B^2}{4\pi\rho_i\nu_{in}} + \eta \right) \frac{4\pi\mathbf{J}}{c} \right]. \quad (4)$$

The Hall term does not affect the time evolution of \mathbf{B} , since $\nabla \times (\mathbf{J} \times \mathbf{B}) \propto -\nabla \times \nabla B^2$ vanishes. Thus, ambipolar diffusion acts as *an additional field-dependent resistivity*. We define the ambipolar diffusion coefficient as

$$\begin{aligned} \lambda_{AD} &\equiv \frac{B^2}{4\pi\rho_i\nu_{in}} \\ &\approx 1.1 \times 10^{17} B_G^2 \left(\frac{n_n}{10^{13} \text{ cm}^{-3}} \right)^{-2} \left(\frac{\chi_i}{10^{-12}} \right)^{-1} \text{ cm}^2 \text{ s}^{-1}, \end{aligned} \quad (5)$$

where B_G means B in gauss.

For our model of the protoplanetary disk, we take the minimum-mass solar nebula of Hayashi (1981). It

is characterized by the surface mass density $\Sigma = \Sigma_0 (R/3 \text{ AU})^{-3/2}$ with $\Sigma_0 = 3.3 \times 10^2 \text{ g cm}^{-2}$, where R is the radial distance from the central star, and the temperature profile given by $T_g = 1.6 \times 10^2 (R/3 \text{ AU})^{-1/2}$. We expect Σ_0 to decrease in time as the nebular gas clears out in the late stage of protoplanetary disk evolution. Hence we use the form $\Sigma_0 = 3.3 \times 10^2 f_\Sigma \text{ g cm}^{-2}$, where f_Σ is an arbitrary parameter less than or equal to unity. If we take the gas to be isothermal, the vertical density profile in hydrostatic equilibrium has a Gaussian form (Kenyon & Hartmann 1987; Chiang & Goldreich 1997, hereafter CG97)

$$n_g = n_0 \exp\left(-\frac{z^2}{2h^2}\right), \quad (6)$$

where $n_0 = \Sigma/(\sqrt{2\pi} m_n h) = 1.4 \times 10^{13} f_\Sigma (R/3 \text{ AU})^{-11/4} \text{ cm}^{-3}$ is the number density of gas in the disk midplane, z is the vertical distance measured from the midplane, and $h \equiv c_s/\Omega$ is the scale height. Here, as usual, $c_s = (kT_g/m_n)^{1/2}$ is the sound speed and Ω is the Keplerian rotation rate. With these values, we can roughly estimate the importance of ambipolar diffusion by taking the ratio of the two coefficients in Eqn. (4):

$$\begin{aligned} \frac{\lambda_{AD}}{\eta} &= \frac{B^2}{4\pi\eta\rho_i v_{in}} \quad (7) \\ &\approx 20 f_\Sigma^{-2} B_G^2 \left(\frac{R}{3 \text{ AU}}\right)^{23/4} \exp\left(\frac{z^2}{h^2}\right). \end{aligned}$$

We note that (1) with a magnetic field sufficiently amplified (up to ~ 1 G), ambipolar diffusion is at least as important as Ohmic dissipation and (2) the ratio has strong spatial dependence within the disk. Remnant magnetism in meteorites suggests that $B \approx 1$ G was typical in the solar nebula. If an efficient dynamo is in action, the ambipolar diffusion term would generally be important in the outer ($R \gtrsim 1$ AU) region of the disk. In the inner region, for a similar value of B and $f_\Sigma = 1$, it is nonnegligible only a few scale heights above and below the midplane, where gas density is much lower. It generally becomes increasingly important as f_Σ decreases.

2.2. Magnetorotational Instability in Protoplanetary Disks

Compared to other astrophysical systems, protoplanetary disks are unusually cold and dense and are therefore associated with very low ionization fractions. Ionization fraction is a key parameter in determining whether a disk will be turbulent or not, since the MRI is confined to regions where the ionization fraction is high enough to ensure good coupling between ions and neutrals. This occurs when the ion-neutral collision rate (ν_{in}) is significantly greater (by 3–100 at least) than the rotation rate (Ω) (Blaes & Balbus 1994; Mac Low et al. 1995; Hawley & Stone 1998). The critical ionization fraction is calculated to be

$$\chi_{crit} = \frac{\Omega}{m_i n_n \gamma} = 2 \times 10^{-12} f_\Sigma^{-1} \left(\frac{R}{3 \text{ AU}}\right)^{5/4} \exp\left(\frac{z^2}{2h^2}\right) \quad (8)$$

(e.g., Balbus & Hawley 1998). Interestingly, this value is only slightly higher than the values of 10^{-12} – 10^{-13} estimated in the bulk of protoplanetary disks (Gammie 1996; Glassgold, Najita, & Igea 1997; Sano et al. 2000).

Many numerical simulations have demonstrated that MRI-induced velocity shears amplify the magnetic field (see, e.g., Hawley & Balbus 1991; Brandenburg et al. 1995; Hawley, Gammie, & Balbus 1995). In our model, perturbations in the magnetic field are also assumed to be generated by the MRI. Considering the low values of χ_i estimated in protoplanetary disks, it is initially unclear whether this assumption is valid or not. Therefore we ask: which region of the solar nebula, if any, is prone to the MRI? (Previous numerical simulations assumed ionization fraction $\chi_i \gg \chi_{crit}$.) This question has been investigated by several authors (Umebayashi 1983; Sano et al. 2000; Fromang, Terquem, & Balbus 2002). Their results are as follows. The ionization fraction is sufficiently high in the innermost region of the disk up to a few tenths of an AU, where the ambient gas temperature is high enough ($T_g \gtrsim 10^3$ K) for collisional ionization to be effective (where it dominates over cosmic ray and radioactive element ionizations; Umebayashi 1983). Also, cosmic rays and stellar X-ray radiation ionize the surface layers (with thickness given by the stopping depth of $\Sigma_a \approx 10^2 \text{ g/cm}^2$) at $R \lesssim 10$ AU and the entire disk at $R \gtrsim 10$ AU, where the surface density of the disk falls below Σ_a . These, then, are the regions where the disk is turbulent, hence effectively transferring angular momentum and also actively accreting. On the other hand, the region near the disk midplane, where terrestrial planets and the asteroid belt now lie, is generally thought to contain no significant heating source and be quiescent, i.e. magnetically dead (radioactive heating is too inefficient to maintain $\chi_i > \chi_{crit}$; see Gammie 1996). These considerations led to the layered accretion model of Gammie (1996; see also Glassgold, Najita, & Igea 1997).

There are two length scales, other than the scale height h , of relevance to this discussion. The wavelength of perturbation most unstable to the MRI is only slightly larger than the critical wavelength at which the instability sets in (BH91) and is given by

$$\lambda_{BH} = \frac{2\pi v_A}{\sqrt{3} \Omega} \approx 0.23 f_\Sigma^{-1/2} B_G \left(\frac{R}{3 \text{ AU}}\right)^{23/8} \exp\left(\frac{z^2}{4h^2}\right) \text{ AU} \quad (9)$$

(BH91). Other processes affect the growth of perturbations: in dense parts of the disk, collisions with neutrals hinder the charged components from drifting with the magnetic field. In this case, Ohmic dissipation acts to stabilize wavelengths shorter than the resistive diffusion scale $\lambda_\Omega \equiv 2\pi\eta/v_A$, where $v_A = B/(4\pi\rho_n)^{1/2}$ is the Alfvén speed. In other words, the critical wavelength at which MRI sets in is given by $\lambda_{crit} = \max(\lambda_{BH}, \lambda_\Omega)$ (Blaes & Balbus 1994; Sano et al. 2000). When $\lambda_\Omega > \lambda_{BH}$, the perturbation growth becomes much slower. An additional constraint enters when λ_{crit} becomes comparable to the scale height h ; at this point, saturation of the MRI is thought to occur (Balbus & Hawley 1998).

Sano et al. (2000) investigated where the MRI operates in protoplanetary disks by including a detailed chemical reaction scheme and the effect of the recombination of ions and electrons on grain surfaces. They showed that for the minimum-mass solar nebula ($f_\Sigma = 1$) the 2–3 AU region of the disk would be stabilized by Ohmic dissipation. However, as the surface density parameter, f_Σ , is

lowered, the unstable region expands (see their Figure 8). Also, as the disk evolves, dust grains settle to a thin layer in the midplane, and so the grain abundance in the bulk of the nebula gradually decreases. For this reason, Sano et al. (2000) introduced a dust depletion factor, f_d , which measures the abundance of dust grains relative to that in molecular clouds. Thus a low value of f_d may correspond to an old, evolved disk. They demonstrated that as f_d decreases for a given surface density, the stable region (the “dead zone”) shrank in size, and for $f_d \lesssim 10^{-2}$, the entire disk becomes unstable for $R > 3$ AU (see their Figure 11). This happens because the recombination rate on grain surfaces decreases. They found a similar trend as grain growth occurs. From these results, we conclude that the region at $R \approx 3$ AU will become magnetically active at a sufficiently late stage of the evolution. We use and discuss this result further in § 3. Figure 1 compares the three relevant length scales at an early (a) and a late stage (b) of solar nebula evolution. The region of interest where magnetic fields amplify due to the MRI extends from 2 AU to 4 AU in (a), while with a reduced gas density, the active region moves inward to 1–2 AU (b).

2.3. Formation of Current Sheets

In this and the following sections, we consider a simple, one-dimensional geometry illustrated in Figure 2. Also shown are the directions of various terms in Eqns. (3) and (4). Consider first a case in which a magnetic null is present. Near the null, a magnetic pressure gradient, $-\nabla(B^2/8\pi)$, acts on ions and pushes the field lines into the null point in both directions. The ion-neutral drift is then directed toward the null. Along a gradient in the magnetic field, this nonlinear term produces faster field diffusion in regions of stronger field, driving field into regions of weaker field and steepening the gradient, rather than spreading it out as the linear Ohmic term does. Ultimately, the gradient sharpens towards a singularity, marked by a sheet of high electric current. This steepening of magnetic field profile (BZ94) occurs within a timescale of $\tau_{AD} \equiv L_{BH}^2/(2\lambda_{AD}) = (\pi^2/6)(\nu_{in}/\Omega^2)$, calculated to be $\pi/12$ of the orbital period when $\chi_i = \chi_{crit}$. The factor of $1/2$ in τ_{AD} takes into account the fact that the characteristic length decreases as steepening proceeds.

Remarkably, this sharpening has been shown to occur even in the absence of nulls due to a variety of processes including a rotating eddy (BZ94; Zweibel & Brandenburg 1997), accretion disks sustaining the MRI (Mac Low et al. 1995), large amplitude Alfvén waves (Suzuki & Sakai 1996), and the nonlinear stage of Wardle C-shocks (Mac Low & Smith 1997). As previously mentioned, we take the example of magnetohydrodynamic turbulence driven by the MRI. In this case, velocity shears produce magnetic nulls and current singularities. Stretched by shear flows, magnetic nulls develop where the magnetic field changes directions. We therefore crudely estimate that the separation between two adjacent magnetic nulls $L_{BH} = \lambda_{BH}/2$.

We note that ambipolar diffusion allows the field to slip through the neutrals and tends to weaken the MRI. For strong enough diffusion, i.e. when the ion-neutral collision rate (ν_{in}) is much higher than the growth rate of the MRI ($\sim \Omega$), the instability is entirely prevented (Mac Low et al. 1995; Hawley & Stone 1998). On the other

hand, ambipolar diffusion is required to generate current sheets. For our model, we use parameters on the interface between the two regimes. This choice is justified by two-dimensional simulations performed by Mac Low et al. (1995), which showed that for drag coefficients γ a few times the minimum value that allows the instability to develop, $\gamma_{min} \equiv \Omega/(m_i n_n \chi_{crit})$, both the instability and ambipolar diffusion sharpening occur. In other words, we require $1 \lesssim \gamma/\gamma_{min} < 100$. Alternatively, magnetic field amplification could have preceded the epoch of current sheet formation.

We now make quantitative estimates of the properties of current sheets. BZ94 showed that, in the absence of resistivity, the magnetic field profile relaxes to $B \propto x^{1/3}$, and the current density $J \propto \partial B/\partial x \propto x^{-2/3}$ becomes singular at the origin. In reality, both the finite resistivity and the ion pressure act to remove this singularity (Brandenburg & Zweibel 1995). Under the physical conditions of protoplanetary disks, ion pressure can be neglected (Heitsch & Zweibel 2003). The induction term in Eqn. (4), $\nabla \times (\mathbf{v} \times \mathbf{B})$, becomes progressively less important as the field steepens; $I/O \approx vL/\eta$ where I and O denote the magnitudes of the induction and Ohmic dissipation term respectively, and is therefore ignored. The quasi-steady-state magnetic field profile (“Quasi” since the magnetic field profile lasts only as long as the velocity shear is present, for about a dynamical time) is calculated by balancing the Ohmic dissipation term against the ambipolar diffusion term in Eqn. (4):

$$(B_0^2 + B_y^2) \frac{d^2 B_y}{dx^2} + 2B_y \left(\frac{dB_y}{dx} \right)^2 = 0. \quad (10)$$

Here, for simplicity, we use the definition

$$B_0 \equiv (4\pi\eta\rho_i\nu_{in})^{1/2} \approx 0.26 n_{g13} T_{g3}^{1/4} \text{ G}, \quad (11)$$

which measures the relative importance of Ohmic dissipation to ambipolar diffusion. We used n_{g13} and T_{g3} to denote $n_g/(10^{13} \text{ cm}^{-3})$ and $T_g/(10^3 \text{ K})$, respectively. Ohmic dissipation dominates where $B < B_0$; ambipolar diffusion wins where $B > B_0$ (see Eqn. 7). Remarkably, B_0 is independent of the ionization fraction; so is the magnetic field profile. Solving Eqn. (10), we obtain

$$\frac{1}{3} B_y^3 + B_0^2 B_y = \Gamma x, \quad (12)$$

assuming that the field vanishes at the origin. An integration constant, Γ , is determined by the boundary condition $B_y(x = L_{BH}) = B_{max}$, which leads to $\Gamma = B_{max}(B_0^2 + B_{max}^2/3)/L_{BH}$. The amplitude of the magnetic field, B_{max} , is determined from the remnant magnetic field strengths recorded in the matrix of chondrites (0.1–1 G) and in chondrules themselves (1–10 G) (Desch & Connolly 2002, and references therein). From Eqn. (12), we see that $B_0^2 \gg B_y^2/3$ near the origin, and the effect of resistivity yields $B_y \approx \Gamma x/B_0^2$. Note the current density singularity is now removed; the maximum current density near the origin is given by $J(x=0) = c\Gamma/4\pi B_0^2$, which is finite. Sufficiently far from the origin where $B_0^2 \ll B_y^2/3$ is satisfied, $B_y \approx (3\Gamma x)^{1/3}$ holds, and we retain the result in the non-resistive limit of BZ94. There, the current density declines steeply ($J \propto x^{-2/3}$). We therefore set $B_0^2 = B_y^2/3$ and compute the width of the current sheet to be

$$l_{cs} = \frac{2\sqrt{3}B_0^3}{\Gamma} \quad (13)$$

$$\approx 1.5 \times 10^5 n_{g13}^{5/2} T_{g3}^{3/4} B_G \left(\frac{B_{max}}{3 \text{ G}} \right)^{-3} \left(\frac{R}{3 \text{ AU}} \right)^{3/2} \text{ km}.$$

This expression is valid for $B_{max} > \sqrt{3} B_0$, which is satisfied under the conditions of interest.

2.4. Heating Mechanisms

Inside current sheets, two heating mechanisms act. First, electrons and ions are accelerated by the electric field present, and then collide with neutrals and heat up the entire gas, leading to familiar Ohmic dissipation. The corresponding heating rate per unit volume essentially follows from the magnetic field profile:

$$\varepsilon_\Omega = \frac{j^2}{\sigma_e} = \frac{\eta}{4\pi} \left(\frac{dB_y}{dx} \right)^2. \quad (14)$$

There is additional heating due to friction when ions, accelerated by the Lorentz force, diffuse through neutrals (see, e.g., § 2.1 of this paper; Padoan, Zweibel, & Nordlund 2000). In this case of ambipolar diffusion heating,

$$\varepsilon_{AD} = \rho_i \nu_{in} |\mathbf{v}_i - \mathbf{v}_n|^2 = \frac{\eta B_y^2}{\pi B_0^2} \left(\frac{dB_y}{dx} \right)^2 \quad (15)$$

yields the volumetric heating rate. Note that their ratio is given simply by $\varepsilon_{AD}/\varepsilon_\Omega = B_y^2/4B_0^2$. Within the range of parameters we are interested in, the ambipolar diffusion heating integrated through the current sheet along x exceeds (by a factor of ~ 10 in our fiducial model) the contribution from Ohmic dissipation.

The resulting heating profiles ($\log \varepsilon$ vs. $\log x$) as a function of B_0 , defined in Eqn. (11), are displayed in Figure 3. They are naturally symmetric around $x = 0$. In terms of shape, these double peaks are similar to what has been observed in numerical simulations of Padoan, Zweibel, & Nordlund (2000), although their sheets are produced by supersonic shocks and density compressions. Ambipolar diffusion sharpening becomes more efficient at lower gas densities (see Eqn. 13), and the current densities become close to singular. This implies stronger and more concentrated heating far above and below the disk midplane. Alternatively, if the disk becomes thinner with time (Ruden 1999), the heating rate also increases. For example, soon after thermonuclear reactions began in the Sun, a powerful solar wind is thought to have blown away the gas ~ 0.1 to a few million years after the solar nebula formed. Accretion onto the central star or, in local regions, planetary accretion as gap formation occurs would have the same effect. A density drop caused by any of these mechanisms introduces a regime where chondrule formation is favored. As the overall gas density n_g drops in time, $B_0 \propto n_g$, so the peak heating rate rises.

3. APPLICATIONS

3.1. Energy Equations and Chondrule Formation

We investigate chondrule heating in current sheets by solving numerically the coupled equations of energy transfer for gas and dust particles, and compare the results with the experimental constraints on chondrule formation.

Dust particles are usually assumed to possess a power-law distribution of sizes with upper and lower size cutoffs (e.g. Chiang et al. 2001). For simplicity, we use just two types of dust particles: small, micron-sized dust grains

with radius $a_d = 1 \mu\text{m}$ and bigger, millimeter-sized chondrules with $a_c = 1 \text{ mm}$. Also, it is assumed that the same amount of mass is contained in each type. Near the dust melting temperature, small grains radiate in the near-infrared most efficiently. Hence their thermal evolution is of considerable importance to the overall development of current sheets.

To study how these current sheets affect the temperatures of dust particles that emit the bulk of the infrared radiation, we use the one-dimensional slab geometry considered in Hood & Horanyi (1993). Dust and gas travel through a current sheet with relative velocity of v_r , where v_r is a free parameter of the model but assumed to be comparable to the Alfvén speed, $v_A = B/(4\pi\rho_n)^{1/2}$, and smaller than 17 km s^{-1} , the Keplerian orbital speed at $R = 3 \text{ AU}$. For our fiducial model, $v_r = 1 \text{ km s}^{-1}$. We discretize the region for computation so that each zone has a thickness of 1 km and we use 10^3 zones. Note that the lateral extent of our computational domain exceeds that of our fiducial current sheet ($l_{cs} \approx 10^2 \text{ km}$). The gas and dust temperatures are uniform in each zone but in general differ from each other. The temperatures evolve in time and are assumed to vary only in one spatial direction (x).

Entering a current sheet, gas molecules gain energy from the two heating mechanisms mentioned in § 2.4 and lose it through collisions with dust grains and chondrules. The collisional heat transfer rate per unit surface area between gas and dust, denoted by q_d , is defined as $q_d = (3/4\sqrt{\pi})(2k/m_n)^{3/2}\rho_g(T_g - T_d)$ and q_c is defined similarly for chondrules (Hood & Horanyi 1993). Then the gas temperature evolves in time according to

$$n_g k \frac{dT_g}{dt} = \varepsilon - \sum_{i=d,c} 4\pi a_i^2 n_i q_i + \rho_g \kappa_{IR} (J_r - 4\sigma T_g^4), \quad (16)$$

where k is the Boltzmann constant, n_i is the number density of either dust grains ($i = d$) or chondrules ($i = c$), and $\varepsilon = \varepsilon_\Omega + \varepsilon_{AD}$. The opacity of the gas, κ_{IR} , is mainly due to dust associated with it, and is set to $1.0 \text{ cm}^2 \text{ g}^{-1}$, appropriate for infrared wavelengths (Chiang et al. 2001). The intensity of radiation, J_r (integrated over all wavelengths) at $x = x_0$ from plane-parallel, temperature-stratified atmospheres has the following form (Mihalas 1978; Desch & Connolly 2002):

$$J_r(x_0) = 2\sigma \int_{-\infty}^{+\infty} (\rho_g \kappa_{IR} T_g^4 + \sum_{i=d,c} n_i \pi a_i^2 \epsilon_i T_i^4) E_1(\beta|x-x_0|) dx \quad (17)$$

with $\beta \equiv \rho_g \kappa_{IR} T_g^4 + \sum_{i=d,c} n_i \pi a_i^2 \epsilon_i$. Here, ϵ_i is the emissivity of a grain of type i averaged over the Planck function at temperature $T_i(x)$, which we simply set at 1.0 (for comparison, Desch & Connolly (2002) uses values of 0.8 and 0.4 for 1 mm- and 1 μm -sized grains, respectively), and E_1 is the exponential integral of the first type. Dust grains and chondrules, on the other hand, are heated both by colliding with hotter gas molecules and by absorbing radiation from nearby smaller, micron-sized, grains which reach high temperatures quickly. They lose energy by radiating an approximate blackbody spectrum at T_d and T_c , with emission efficiency of ϵ_d and ϵ_c for dust and chondrules, respectively. Therefore,

$$m_i C_i \frac{dT_i}{dt} = \pi a_i^2 [4q_i + \epsilon_i (J_r - 4\sigma T_i^4)]. \quad (18)$$

As before, the index i can be either d (for dust) or c (for chondrule). The last term in Eqn. (18) represents the incident flux on a given particle radiated by dust grains in the other zones minus its own emission.

The experimental constraints on chondrule formation are (1) the grains are completely melted for a few minutes; (2) the cooling timescale of gas and dust is approximately an hour, consistent with the oft-quoted value of 10^2 – 10^3 K hr^{-1} ; and (3) small grains ($\lesssim 0.1$ mm) are absent, possibly evaporated or destroyed completely after passing through a current sheet, leading to the observed narrow size distribution centered at $a_d \approx 1$ mm.

From the properties of current sheets described in § 2.3–2.4, we infer that the above constraints on chondrule formation will be satisfied only if the following conditions are met:

(1) In order to obtain high enough heating rate, the gas density has to be low ($n_g \lesssim 10^{12}$ cm^{-3}), because the heating rate increases steeply as n_g decreases.

(2) To have "localized" heating events, spatially averaged chondrule/dust densities should be high ($n_d > 1$ cm^{-3}). Otherwise, the mean free path for IR photons will exceed a few hundred kilometers and the heating timescale will be much more than "a few minutes."

(3) To ensure good thermal coupling between gas and dust, either the gas density has to be high ($n_g \gtrsim 10^{12}$ cm^{-3}) because $q_d, q_c \propto n_g$ which cannot be satisfied because of the first condition, or dust grains need to be very small ($a_d \lesssim 1$ μm) so they approach T_g quickly.

In order to satisfy conditions (1)–(3) simultaneously, the dust-to-gas mass ratio, ζ , should be very large, about 50. Usually $\zeta \approx 0.01$ is assumed for the minimum amount solar nebula, but after a few million years the gas density is expected to have decreased due to viscous diffusion (Ruden & Lin 1986) as well as the various mechanisms mentioned in the last paragraph of § 2.4. Dust settles into a thin, dense layer on a timescale $\tau_s \approx (a/1 \mu\text{m})^{-1} f_\Sigma$ Myr, independent of R (Ruden 1999, CG97), comparable to the lifetimes of protoplanetary disks. There will still be some dust grains, particularly submicron-sized ones, that remain well above the midplane mixed with the gas. But at late times the dust outside the thin, dense dust layer is likely to be quite small, decreasing the dust-to-gas ratio there. Inside the dust layer, however, solids may dominate the local density (Cuzzi, Dobrovolskis, & Champney 1993). Hence, $\zeta \approx 50$ may be reached in the midplane, where most solids reside.

We solve Eqns. (16)–(18) simultaneously for $T_g(x, t)$, $T_d(x, t)$, and $T_c(x, t)$ using a fifth-order Runge-Kutta scheme appropriate for a stiff set of equations with adaptive stepsize control (Press et al. 1992). Both gas and dust particles begin at the same temperature, $T_{init} = 500$ K. The center of a current sheet is initially placed at $x = 1000$ km and moves to the left at v_r . To simplify the problem, we ignore the time evolution of ε and χ_i (see § 4). For our fiducial model, $n_g = 10^{12}$ cm^{-3} and both n_d and n_c are set to yield desired values of the dust-to-gas ratio ζ .

3.2. Results

Figure 4 shows the time evolution of gas, dust, and chondrule temperatures at a fixed position as a current sheet moves through, for our model runs with $\zeta = (5, 50)$. We

also ran the code for $\zeta = 0.05$ but do not plot the result because both T_d and T_c remain practically unchanged at T_{init} for over 10^3 s. We find that for $\zeta = 5$ the gas temperature rises appreciably (above 1000 K) but, due to poor thermal coupling between gas and dust, neither T_d nor T_c changes significantly, reaching only ~ 700 K after 10^3 s. In the run with $\zeta = 50$, however, due to the increase in optical depth, dust grains follow the gas temperature closely and the radiation field also steadily increases in strength. The grains melt after about 570 seconds and evaporate after about 630 seconds, at which point we stop the simulation, as it does not take into account the evaporation of particles. We changed the boundary condition between flat at T_{init} and a floating boundary condition but found the result remained qualitatively the same. In an improved model that accounts for evaporation and a range of dust grain sizes, we expect the smallest grains to evaporate first, decreasing the optical depth, thus widening the heated region and lowering the net volumetric heating rate. The larger grains will therefore probably not evaporate. This is interesting since it could naturally explain the peaking of the size distribution of chondrules around 1 mm.

The fact that chondrules get melted only for high values of ζ is consistent with the FeO record in chondrules, which seems to indicate oxygen fugacities (relative abundance of oxygen to hydrogen) at formation that are higher than solar values by at least two or three orders of magnitude (Wood 1967). This is most often interpreted to mean that chondrules were heated in regions with extremely high dust-to-gas ratios. The dust is taken to be oxides of Si, Mg, Ca, Al, etc. in chondritic proportions which bring in a large amount of oxygen. For this reason also, it is advantageous to evaporate the smaller grains first because then oxides will be incorporated into the gas and the partial pressures of condensable elements will increase locally. This helps to make liquids stable at high temperature, and also suppresses the evaporation of silicate liquids which would have caused heavy isotope enrichment of resulting chondrules; such enrichment is not observed (Galy, Young, Ash, & O’Nions 2000). Ebel & Grossman (2000) gives a full treatment of what dust enrichments are necessary to make FeO-bearing silicates and also to make chondrule liquids stable at low pressure relative to solids, as well as a discussion of dust-enrichment scenarios with high oxygen fugacities. The idea that the midplane is a better place to consider chondrule formation is supported again in this context.

The value of the gas density used in Figure 4 is $n_g = 10^{12}$ cm^{-3} corresponding to $f_\Sigma = 10^{-1}$. Since we expect the gas density in the disk to decrease to this level after a time of order a few million years, this argues for chondrule formation in a late, evolved disk, and is consistent with the age difference between CAIs (refractory Ca-Al-rich inclusions) and chondrules, estimated from the decay of ^{26}Al (with a half-life of 0.7 Myr) to be 2–3 Myr (Hutcheon et al. 1994; Russell 1996; Swindle et al. 1996).

3.3. Current Sheets in the Disk Midplane

From the results in the previous section, we conclude that in a standard model of the early solar nebula in which dust and gas are well-mixed, the disk will have $\zeta \approx 0.01$ everywhere and hence heating of dust grains by current

sheets will not be effective. This conclusion no longer holds in the late stage of the disk evolution. As argued by Sano et al. (2000), the bulk of the disk becomes unstable to the MRI, therefore susceptible to current sheet formation, for low enough values of the surface density factor f_Σ or of the dust depletion factor f_d because the recombination rate on grain surfaces decreases and thus χ_i rises except in a thin layer around the midplane. Current sheets capable of melting mm-sized dust grains form only when $n_g < 10^{12} \text{ cm}^{-3}$ and ζ is quite high, i.e. near the disk midplane. For these reasons, we henceforth consider a late stage of solar nebula evolution in which the gaseous disk has depleted by a factor of 10 ($f_\Sigma = 10^{-1}$) and settling of dust grains onto the midplane has proceeded significantly ($f_d \leq 10^{-2}$).

Let us first estimate the thickness of this dust-rich layer. We assume that ζ has increased from the well-mixed value of 10^{-2} to 50. Taking into account the reduction in gas density, the vertical scale height of dust grains is expected to decrease by a factor of 500 compared to the gas scale height of 0.1 AU at $R = 2$ AU. Thus a thickness of 3×10^4 km is estimated. This thin dust-rich layer around the midplane will be mostly magnetically dead because of the extremely high dust density there, and the resulting high recombination rate on grain surfaces (Sano et al. 2000). Yet, the thin surfaces of this dust layer will be sufficiently ionized by cosmic rays and stellar X-ray radiation to support the MRI and generate current sheets, considering that there are now few dust grains suspended in the upper atmosphere. Current sheets that form in these thin layers will ionize nearby regions within the dust layer, into optical depth of order unity. Dust grains are heated after passing through these current sheets, sometimes up to their melting temperature ($T_{melt} \approx 1600$ K) as shown in § 3.1, and then radiate strongly in the near-infrared, subsequently raising the temperature of dust grains in the surrounding environment. Collisions with hot dust grains may then ionize⁴ the gas in an initially magnetically dead area above the critical value, χ_{crit} .

However, the integrated optical depth of the protosolar nebula at $R = 2$ AU to the near-infrared radiation in the vertical direction is estimated to be $\tau = \kappa_{IR}\Sigma \approx 2 \times 10^2$ (D'Alessio, Calvet, & Hartmann 2001; Chiang et al. 2001). Even if we assume that some of the smallest, submicron-sized grains have been removed from the nebula with the gas, the magnetically active region affected by current sheets would still be only a few percent of the dust-rich layer. To melt the majority of the dust grains that reside in the midplane and form chondrules, the entire layer must be in motion so that all dust particles are exposed in the magnetically active surface layer at some point.

When most of the solids have settled to the midplane, vertical shear between the gas and the differentially rotating, dense particle layer can drive turbulence within a 10^4 – 10^5 km thick boundary layer (Cuzzi, Dobrovolskis, & Champney 1993; Cuzzi, Dobrovolskis, & Hogan 1996). Although vertical velocity gradients vanish by symmetry very near the midplane, a turbulence model that self-consistently deals with generation, transport, and damp-

ing shows that the turbulence diffuses inward and persists even very near the midplane (Cuzzi, Dobrovolskis, & Champney 1993, and references therein)⁵. We take a typical velocity of $U \approx 10^2 \text{ cm s}^{-1}$ [see Eqn. (65) of the previous reference] and the thickness of the dust layer, $L_d \approx 3 \times 10^4$ km, and estimate the eddy turnover time to be $L_d/U \approx 1$ yr. Keeping in mind that the fraction of current sheets covering the dust surface is quite small ($l_{cs}/L_{BH} \approx 3 \times 10^{-5}$; see the next subsection), we expect an average dust grain to be exposed to current sheet heating about once every 3×10^4 yrs. After the brief heating, now spherical, mm-sized chondrules will settle down to the midplane, collecting rims of dust in the process. Such rims are observed (Metzler & Bischoff 1996, and references therein).

3.4. Near-Infrared Excesses

The higher than predicted flux at 2–8 μm observed in the spectra of some young protoplanetary disks has been known for a decade (Hartmann, Kenyon, & Calvet 1993; Natta et al. 1999; Chiang et al. 2001). Using a disk model that included an accounting of grain size distributions and grain compositions, and numerical solution of the equations of radiative and hydrostatic equilibrium under the two-layer approximation of CG97, Chiang et al. (2001) rediscovered this in 4 of their 5 Herbig Ae and T Tauri stars, and found a relative dearth of emission shortward of 10 μm arising partly from low absorption efficiencies of silicate grains. It is noteworthy that these sources also showed evidence for dust settling; parameters appropriate for gas and dust that are well-mixed in interstellar proportions did not fit the overall level of infrared excess at $\lambda \lesssim 100 \mu\text{m}$ for 4 of them. They interpreted this to mean that dust in disk surface layers has settled vertically towards the midplane.

Dullemond, Dominik, & Natta (2001) proposed a disk model in which an inner rim located at the dust evaporation radius forms a vertical wall due to direct heating by the central star and, as a result, puffs up and intersects more starlight. Its reemitted flux produces a bump that peaks at 2–3 μm in the SED. They note that this modification would be significant only for Herbig Ae stars. This mechanism works only if optical depth due to gas opacity in the inner hole is negligible, but in fact it is quite large, of order 10^3 , when a standard surface mass density profile $\Sigma \propto R^{-3/2}$ is assumed, although the surface density of the inner disk is not constrained by the data (Natta et al. 2001).

We suggest an alternative mechanism by noting that current sheets at the dust melting temperature would radiate at just the right wavelengths to fill in the deficient flux at 2–8 μm , perhaps explaining the excess near-IR fluxes. A simple estimate can be made as follows. We take the mean separation between current sheets (produced by the Brandenburg-Zweibel mechanism) to be $L_{BH} = \lambda_{BH}/2$, roughly the distance between two adjacent magnetic nulls produced by the MRI. The total emission from dust grains

⁴ The dominant ion species in protoplanetary disks are alkali metals (Na^+ , K^+). Grains are dominant charge carriers at $T_g \lesssim 10^3$ K, but at higher T_g desorption of charged ions from the surface of dust grains becomes effective (Umebayashi 1983). Thus, our neglect of the effect of charged dust grains is partially justified, at least inside current sheets.

⁵ But see Sekiya (1998) and Youdin & Shu (2002) for claims that turbulent mixing becomes ineffective if the dust-to-gas surface mass ratio is significantly enhanced.

inside current sheets is given by (Chiang et al. 2001)

$$L_\lambda \approx \frac{l_{cs}}{L_{BH}} \left[8\pi^2 \lambda \int_{1 \text{ AU}}^{2 \text{ AU}} 2 B_\lambda(T_{melt}) R dR \right] \\ \approx 10^{32} \left(\frac{\lambda_\mu^4 [\exp(9/\lambda_\mu) - 1]}{2 \times 10^3} \right)^{-1} \text{ erg s}^{-1}, \quad (19)$$

for $n_g = 10^{12} \text{ cm}^{-3}$ at $R = 3 \text{ AU}$. Here, λ_μ is the wavelength of radiation in microns. Taking $l_{cs} \approx 10^2 \text{ km}$ and $L_{BH} \approx 0.03 \text{ AU}$, we obtain $l_{cs}/L_{BH} \approx 3 \times 10^{-5}$ for the fraction covered by current sheets in the region between 1 and 2 AU, the site of their formation in an evolved disk thinned by $f_\Sigma = 10^{-1}$ (see Figure 1b). This crude estimate for the excess near-IR emission from current sheets may partly explain the observed excesses in the range of 10^{32} – $10^{33} \text{ erg s}^{-1}$. Uncertainties in modeling of protoplanetary disks at present are admittedly large. Our mechanism involving current sheets could be taken as an example of producing near-IR excesses when magnetohydrodynamical effects are considered.

Ultimately, these ideas can be tested by searching for distinguishable observable signatures using techniques that have recently emerged. Interferometric imaging of LkH α in the H and K bands by Tuthill, Monnier, & Danchi (2001) has shown a central gap (or cavity) and a hot inner edge, observed at 3.4 AU from the central star when a distance of 160 pc to LkH α is assumed. Earlier theoretical predictions for its radius to fit the near-IR inflections in the SED ($\sim 10R_*$; Hillenbrand et al. 1992) are too small by around an order of magnitude. If we can divide the disk into several annular regions and obtain photometric measurements of each annulus, we suggest that there would be a local maximum of near-IR radiation between 1 and 2 AU, for systems like our primordial solar nebula (although for other young stellar objects, the exact position will depend on stellar and disk parameters and should be recalculated). In standard protoplanetary disk models such as CG97, the mentioned region reaches temperatures of only 100–400 K and is expected to emit poorly in the near-IR. In the near future, a multi-band, adaptive optics coronagraph under development at the American Museum of Natural History (Oppenheimer 2000) will be used to directly view protoplanetary disks and will present another possibility to test these theories.

4. CAVEATS

Our conclusions suffer from several caveats. All models of the current sheets that have been done to date have assumed a steady state flow (BZ94; Brandenburg & Zweibel 1995; Zweibel & Brandenburg 1997; Heitsch & Zweibel 2003). However, the heating and ionization that occur in the current sheet are not accounted for self-consistently in these models. Both will increase the ion pressure in the center of the sheet, either saturating the singularity or even blowing the sheet apart. Also, we invoke turbulence induced by the MRI when calculating magnetic field fluctuations but ignore its effect on the evolution of current sheets, e.g. the converging motion of the neutrals in ambipolar diffusion. In our simplified chondrule formation model, we let gas and dust travel through a current sheet at $v_r \approx 1 \text{ km s}^{-1}$, but it is not clear how well this approximates the actual condition near a current sheet or if a

current sheet would survive in that environment. To study these effects in detail a dynamical model will be necessary. This requires modeling the interplay between at least four physical processes: pressure imbalance, ionization evolution, temperature evolution, and steepening of the magnetic field. These four processes are inherently connected and feed back on one another. That means they must be solved simultaneously in a self-consistent fashion. Radiative transfer and a power-law size distribution of dust grains must be incorporated in a subsequent step to understand chondrule formation in these dynamical models. The large range of timescales and length scales involved presents another challenge for modeling of this complicated set of processes.

We are grateful to Axel Brandenburg, Eugene Chiang, Fabian Heitsch, and Ellen Zweibel for helpful discussions, as well as an anonymous reviewer of an NSF grant proposal for pointing out the importance of high oxygen fugacities derived for chondrules. M. K. R. J. was supported by an AMNH Graduate Student Fellowship. M.-M. M. L. acknowledges support by NSF Career grant AST99-85392, NSF grant AST03-07793, and NASA ATP grant NAG5-10103. D. S. E. acknowledges support from NASA Cosmochemistry grant NAG5-12855.

REFERENCES

- Adams, F. C., Lada, C. J., & Shu, F. H. 1987, *ApJ*, 312, 788
- Balbus, S. A., & Hawley, J. F., 1991, *ApJ*, 376, 214 (BH91)
- Balbus, S. A., & Hawley, J. F., 1998, *Rev. Mod. Phys.*, 70, 1
- Balbus, S. A., & Terquem, C., 2001, *ApJ*, 552, 235
- Beckwith, S. V. W., Sargent, A. I., Chini, R. S., & Gusten, R. 1990, *AJ*, 99, 924
- Blaes O. M., & Balbus S. A., 1994, *ApJ*, 421, 163
- Boss A. P. 1996, *Chondrules and the Protoplanetary Disk*, eds. R. H. Hewins, R. H. Jones, & E. R. D. Scott (Cambridge: Cambridge Univ. Press), 257
- Brandenburg, A., Nordlund, A., Stein, R. F., & Torkelsson, U. 1995, *ApJ*, 446, 741
- Brandenburg, A., & Zweibel, E. G. 1994, *ApJ*, 427, L91 (BZ94)
- Brandenburg, A., & Zweibel, E. G. 1995, *ApJ*, 448, 734
- Calvet, N., Hartmann, L., & Strom, S. E. 2000, in *Protostars and Planets IV*, eds. V. Mannings, A. P. Boss, & S. S. Russell (Tucson: Univ. Arizona Press), 377-399
- Chiang, E. I., & Goldreich, P. 1997, *ApJ*, 490, 368 (CG97)
- Chiang, E. I., Joungh, M. K., Creech-Eakman, M. J., Qi, C., Kessler, E. J., Blake, G. A., & van Dishoeck, E. F. 2001, *ApJ*, 547, 1077
- Connolly, H. C., & Love, S. G. 1998, *Science*, 280, 62
- Cuzzi, J. N., Dobrovolskis, A. R., & Champney, J. M. 1993, *Icarus*, 106, 102
- Cuzzi, J. N., Dobrovolskis, A. R., & Hogan, R. C. 1996, *Chondrules and the Protoplanetary Disk*, eds. R. H. Hewins, R. H. Jones, & E. R. D. Scott (Cambridge: Cambridge Univ. Press), 35
- D'Alessio, P., Calvet, N., & Hartmann, L. 2001, *ApJ*, 553, 321
- Desch, S. J., & Connolly, H. C. 2002, *Meteorit. Planet. Sci.*, 37, 183
- Draine, B. T., Roberge, W. R., & Dalgarno, A. 1983, *ApJ*, 264, 485
- Dullemond, C. P., Dominik, C., & Natta, A. 2001, *ApJ*, 560, 957
- Ebel, D. S., & Grossman, L. 2000, *Geochim. Cosmochim. Acta*, 64, 339
- Elmegreen, B. G. 1985, *ApJ*, 299, 196
- Fromang, S., Terquem, C., & Balbus, S. A. 2002, *MNRAS*, 329, 18
- Galy, A., Young, E. D., Ash, R. D., & O'Nions, R. K. 2000, *Science*, 290, 1751
- Gammie, C. F., 1996, *ApJ*, 457, 355
- Glassgold, A. E., Najita, J., & Igea, J. 1997, *ApJ*, 480, 344
- Goldsmith, P. F., & Langer, W. D. 1978, *ApJ*, 222, 881
- Hawley, J. F., & Balbus, S. A. 1991, *ApJ*, 376, 223 (BH91)
- Hawley, J. F., Gammie, C. F., & Balbus, S. A. 1995, *ApJ*, 440, 742
- Hawley, J. F., & Stone, J. M. 1998, *ApJ*, 501, 758
- Hartmann, L., Kenyon, S. J., & Calvet, N. 1993, *ApJ*, 407, 219
- Hayashi, C. 1981, *Prog. Theor. Phys. Suppl.*, 70, 35
- Heitsch, F., & Zweibel, E. G. 2003, *ApJ*, 583, 229
- Hewins, R. H. 1996, *Chondrules and the Protoplanetary Disk*, eds. R. H. Hewins, R. H. Jones, & E. R. D. Scott (Cambridge: Cambridge Univ. Press), 3
- Hewins, R. H. 1997, *Annu. Rev. Earth Planet. Sci.*, 25, 61
- Hillenbrand, L. A., Strom, S. E., Vrba, F. J., & Keene, J. 1992, *ApJ*, 397, 613
- Hood, L. L., & Horanyi, M. 1993, *Icarus*, 93, 259
- Howard, E. Phil. 1802, *Trans. Royal Soc. London*, 92, 168
- Hutcheon, R., Huss, G. R., & Wasserburg, G. J. 1994, *Lunar Planet. Sci.*, 25, 587
- Kenyon, S. J., & Hartmann, L. 1987, *ApJ*, 323, 71
- Krall, N. A., & Trivelpiece, A. W. 1973, *Principles of Plasma Physics* (New York: McGraw Hill)
- Lofgren, G., & Lanier, A. B. 1990, *Geochim. Cosmochim. Acta*, 54, 3537
- Mac Low, M.-M., Norman, M. L., Königl, A., & Wardle, M. 1995, *ApJ*, 442, 726
- Mac Low, M.-M., & Smith, M. D. 1997, *ApJ*, 491, 596
- Mendoza, E. E. V. 1968, *ApJ*, 151, 977
- Mestel, L., & Spitzer, L. S. 1956, *MNRAS*, 116, 505
- Metzler, K., & Bischoff, A. 1996, *Chondrules and the Protoplanetary Disk*, eds. R. H. Hewins, R. H. Jones, & E. R. D. Scott (Cambridge: Cambridge Univ. Press), 153
- Mihalas, D. 1978, *Stellar Atmospheres* (San Francisco: W. H. Freeman & Co.), 650
- Natta, A., Prusti, T., Thi, W. F., Grinin, V. P., & Mannings, V. 1999, *A&A*, 350, 541
- Natta, A., Prusti, T., Neri, R., Grinin, V. P., & Mannings, V. 2001, *A&A*, 371, 186
- Oppenheimer, B. R., Dekany, R. G., Hayward, T. L., Brandl, B., Troy, M., & Bloemhof, E. E. 2000, *Proc. SPIE*, 4007, 899
- Padoan, P., Zweibel, E. G., & Nordlund, Å. 2000, *ApJ*, 540, 332
- Press, W. H., Teukolsky, S. A., Vetterling, W. T., & Flannery, B. P. 1992, *Numerical Recipes in Fortran* (Cambridge: Cambridge Univ. Press)
- Radomsky, P. M., & Hewins, R. H. 1990, *Geochim. Cosmochim. Acta*, 54, 3475
- Ruden, S. P., & Lin, D. N. C. 1996, *ApJ*, 308, 883
- Ruden, S. P. 1999, *The Origins of Stars and Planetary Systems*, eds. C. J. Lada and N.D. Kylafis (Dordrecht: Kluwer), 643
- Russell, S. S., Srinivasan, G., Huss, G. R., Wasserburg, G. J. & MacPherson, G. J. 1996, *Science*, 273, 757
- Sano, T., Miyama, S. M., Umabayashi, T., & Nakano, T. 2000, *ApJ*, 543, 486
- Scalo, J. M. 1977, *ApJ*, 213, 705
- Sekiya, M. 1998, *Icarus*, 133, 298
- Shu, F. H., Adams, F. C., & Lizano, S. 1987, *ARA&A*, 25, 23
- Suzuki, M., & Sakai, J.-I. 1996, *ApJ*, 465, 393
- Swindle, T. D., Davis, A. M., Hohenberg, C. M., MacPherson, G. J., & Nyquist, L. E. 1996, *Chondrules and the Protoplanetary Disk*, eds. R. H. Hewins, R. H. Jones, & E. R. D. Scott (Cambridge: Cambridge Univ. Press), 77
- Tuthill, P. G., Monnier, J. D., & Danchi, W. C. 2001, *Nature*, 409, 1012
- Umabayashi, T. 1983, *Prog. Theor. Phys.*, 69, 480
- Wood, J. A. 1967, *Geochim. Cosmochim. Acta*, 31, 2095
- Wood, J. A. 1996, *Chondrules and the Protoplanetary Disk*, eds. R. H. Hewins, R. H. Jones, & E. R. D. Scott (Cambridge: Cambridge Univ. Press), 55
- Youdin, A. N., & Shu, F. H. 2002, *ApJ*, 580, 494
- Zweibel, E. G., & Brandenburg, A. 1997, *ApJ*, 478, 563
- Zweibel, E. G., & Josafatsson, K. 1983, *ApJ*, 270, 511

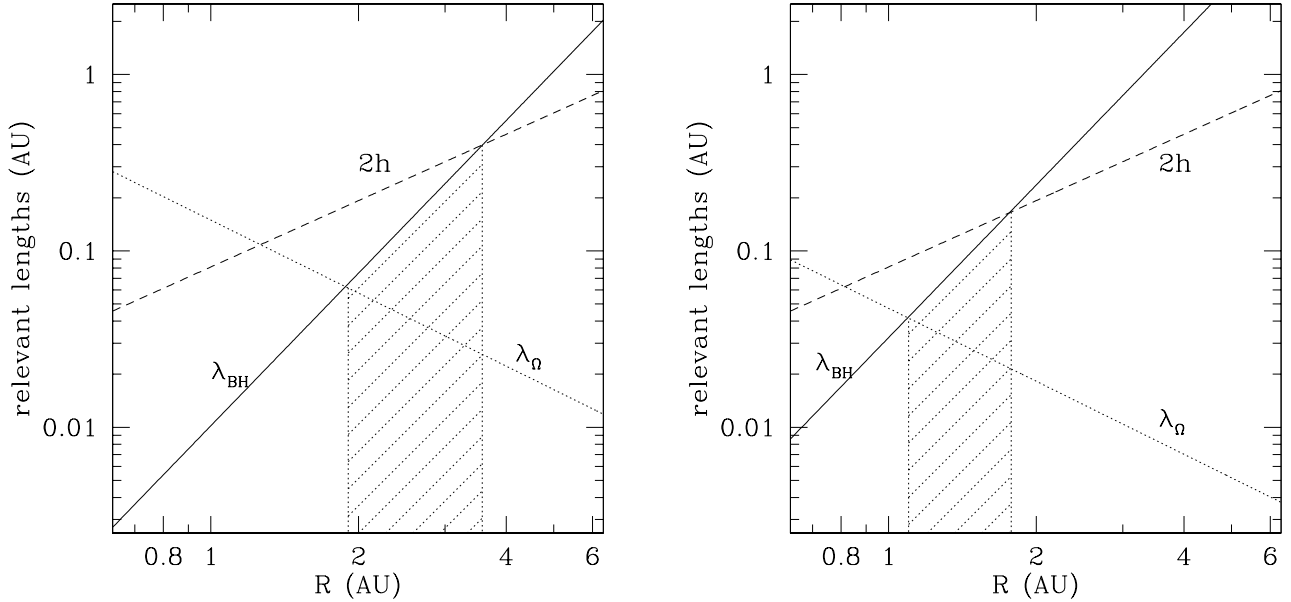


FIG. 1.— Relevant length scales. (a) Assumed parameter values are $f_{\Sigma} = 1$, $B = 1$ G, and $\chi_i = 10^{-12}$. The critical wavelength of the MRI, resistive diffusion scale, and (twice) the scale height of the disk are shown as solid, dotted, and dashed lines, respectively. See text for their definitions. The shaded region satisfying $\lambda_{\Omega} < \lambda_{BH} < 2h$, where the MRI occurs, extends from 2 AU to 4 AU. (b) Same as (a) but using $f_{\Sigma} = 10^{-1}$. This is appropriate for a late stage of the solar nebula evolution. Note that the magnetically active region moves inward to 1–2 AU.

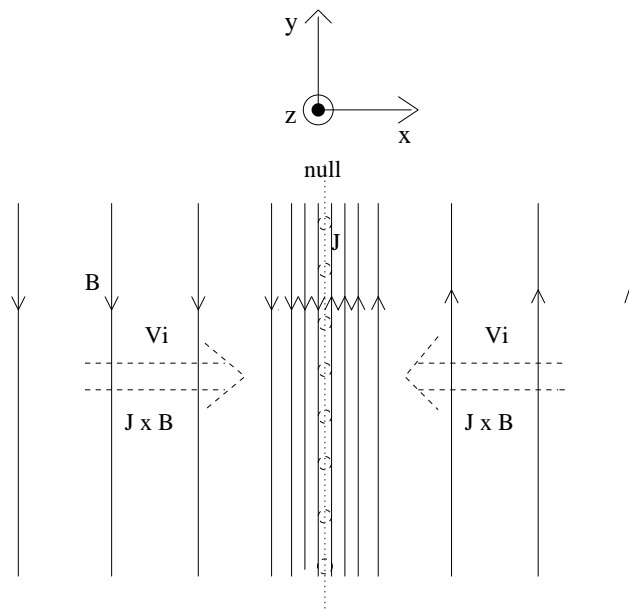


FIG. 2.— Configuration for magnetic fields in the one-dimensional geometry considered in this paper. Current density (J) points in the $+z$ direction, out of the page. The directions of various terms in Eqns. (3) and (4) are also shown. A current sheet forms along the magnetic null, shown as a dotted vertical line along the center of the figure.

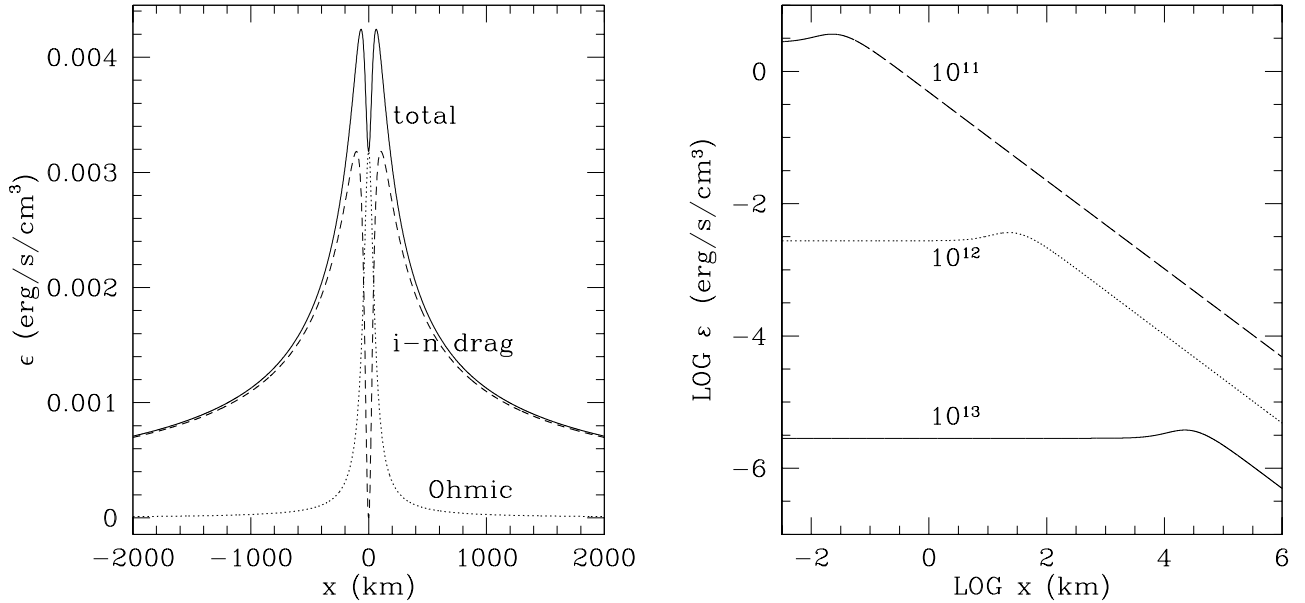


FIG. 3.— (a) Heating profile for our fiducial model with $f_{\Sigma} = 0.1$. Note the symmetry about $x = 0$. Ohmic dissipation (dotted line) is concentrated near center of current sheet, while the ambipolar diffusion heating (dashed line) is centered off-peak. The latter exceeds the contribution from the former by a factor of ~ 6 in our fiducial model. (b) Heating profiles as a function of B_0 in a log-log scale. In this case, the gas density (n_g) was varied, and each curve is labeled with the corresponding value of n_g used. The peak heating rate increases approximately inversely proportional to the square of gas density; the width of current sheet varies as described by Eqn. (13).

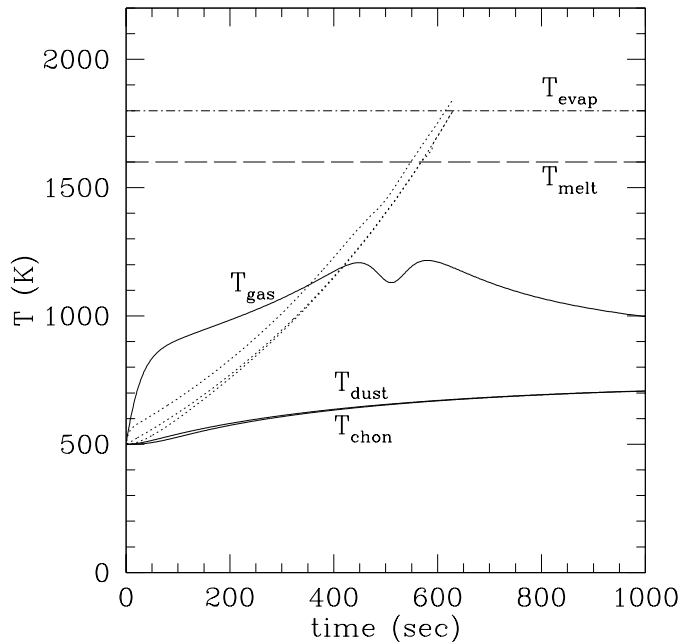


FIG. 4.— Time evolution of gas, dust, and chondrule temperatures at a fixed position in space. Common parameters used for the two runs are: $n_g = 10^{12} \text{ cm}^{-3}$, $a_d = 1 \mu\text{m}$, $a_c = 1 \text{ mm}$, and $B_{max} = 3 \text{ G}$. Solid lines are used for the run with $\zeta = 5$ and dotted lines for the run with $\zeta = 50$. Only for the higher value of ζ do dust grains and chondrules reach the melting temperature. We stop running the code when the particles evaporate. The initially steep rise in T_{gas} is due to initial conditions that are not set self-consistently.